

# Ultra-low-loss CMOS-Compatible Waveguide Crossing Arrays Based on Multimode Bloch Waves and Imaginary Coupling

Yangyang Liu, Jeffrey M. Shainline, Xiaoge Zeng and Miloš A. Popović<sup>1</sup>

<sup>1</sup>*Department of Electrical, Computer, and Energy Engineering,  
University of Colorado, Boulder, CO 80309, USA*

compiled: July 16, 2018

We experimentally demonstrate broadband waveguide crossing arrays showing ultra low loss down to 0.04 dB/crossing (0.9%), matching theory, and crosstalk suppression over 35 dB, in a CMOS-compatible geometry. The principle of operation is the tailored excitation of a low-loss spatial Bloch wave formed by matching the periodicity of the crossing array to the difference in propagation constants of the 1<sup>st</sup>- and 3<sup>rd</sup>-order TE-like modes of a multimode silicon waveguide. Radiative scattering at the crossing points acts like a periodic imaginary-permittivity perturbation that couples two supermodes, which results in imaginary (radiative) propagation-constant splitting and gives rise to a low-loss, unidirectional breathing Bloch wave. This type of crossing array provides a robust implementation of a key component enabling dense photonic integration.

*OCIS codes:* (230.7370) Waveguides; (130.3120) Integrated optics devices.  
<http://dx.doi.org/10.1364/XX.99.099999>

Silicon photonics is beginning to enable complex on-chip optical networks comprising hundreds of devices. One emerging application is energy efficient, chip-scale photonic interconnects for CPU-to-memory communication [1]. With increasing device density and complexity in a planar photonic circuit, efficient waveguide crossings are indispensable in many network topologies [1]. Crossing designs based on adiabatic aperture widening are large and relatively lossy (0.3–1 dB) [2–4], while resonant designs permit low loss and crosstalk in a compact footprint, but have narrow bandwidth [5] (e.g.  $\sim 4$  nm [6]). Multilayer processes allow reduced scattering in crossing waveguides [7] or their complete isolation through vertical displacement [8], but they require multiple lithographic steps and/or material layers. Multimode-interference (MMI) based crossings [9–14], despite ostensibly multimode behavior, have a number of attractive features, with individual crossings down to 0.18 dB loss and 41 dB crosstalk [14].

In this Letter, we describe ultra-low-loss waveguide crossing arrays based on a periodic multimode structure. Popović *et al.* [12] proposed an efficient approach to design a crossing array (Fig. 1) by constructing a low-loss Bloch wave in a matched periodic structure where the optical field synthesizes periodic foci that jump across gaps and avoid diffraction loss and scattering at the crossing points. This concept is reminiscent of periodic lens-array microwave beam guiding [15]. Microphotonic implementations use a minimum of modes to implement focusing physics, eliminate reflections, and introduce new degrees of freedom. In the first experimental demonstration of this concept [16], we showed record low waveguide-crossing loss of 0.04 dB/crossing (0.9%), equal to theoretical design efficiency [12]. Another recent paper [17] demonstrated similar crossing arrays based on our proposal in Ref. 12,

achieving 0.14 dB loss, and introduced an improvement based on subwavelength patterning of the sidewalls, reducing the loss further to below 0.02 dB. To our knowledge, these two results represent respectively the lowest achieved crossing loss in CMOS-compatible photolithography processes [16] and in high-resolution processes allowing nanopatterning, such as scanning electron-beam lithography [17]. In this paper, we present the low-loss unidirectional Bloch mode concept, its use in design of waveguide crossing arrays, and our experimental results on record loss in CMOS-compatible crossings. We show an excellent match between theory and experiment.

The basic concept is similar to MMI-based [10, 11] synthesis of fields that focus across a waveguide crossing region [9] to prevent diffraction loss, extended to an open-system periodic array. The periodicity gives rise to a unique, novel type of Bloch wave formed from two forward propagating modes of different transverse spatial order, which we can refer to as a unidirectional Bloch wave (Fig. 2). This Bloch wave differs from typical Bloch waves formed in photonic crystals by periodic coupling in that the half-wave periodicity of the PhC structure leads to bandgaps at the edges of the Brillouin zone, formed by an anticrossing between the dispersion curves of a forward and a backward guided mode. In

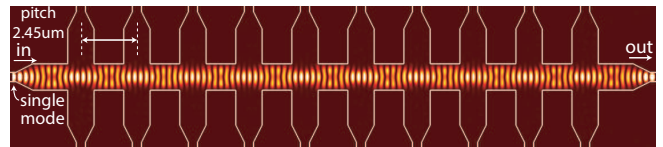


Fig. 1: Ultra-low-loss waveguide crossing array, based on excitation of a low-loss breathing Bloch wave, formed of 1<sup>st</sup> and 3<sup>rd</sup> modes of a multimode waveguide (2D FDTD simulation) [12]. The mode is stabilized by radiative loss.

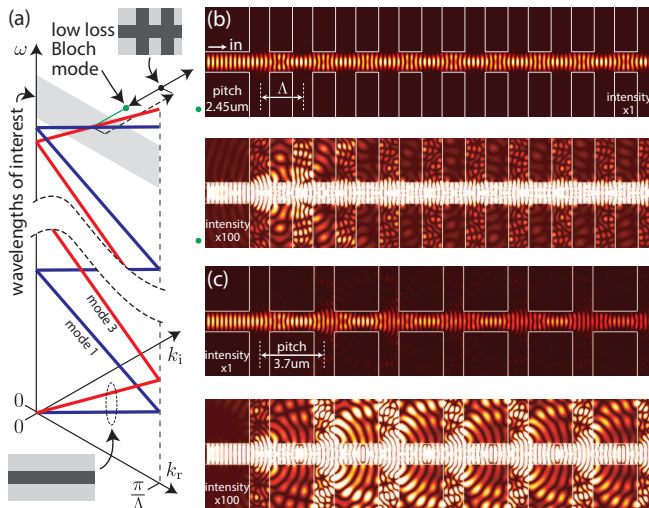


Fig. 2: Unidirectional low-loss Bloch modes: (a) illustration of complex- $k$  band structure of unperturbed waveguide and imaginary- $k$  splitting due to radiative crossings; (b) low-loss breathing field due to matching periodicities of the structure and of the breathing optical field [2D FDTD; bottom: 100x oversaturated intensity to show detail, green dot in (a)] [12]; (c) high propagation loss with mismatched structure and breathing mode periodicities.

the present case, the periodicity leads to an anticrossing of a high order, between forward fundamental and third-order modes, which can be anywhere within the Brillouin zone [Fig. 2(a)]. In this sense, the crossing array is more analogous to a long-period (fiber) grating than a photonic crystal. The typical Brillouin-zone edge bandgap that is the key characteristic of photonic crystals will be primarily absent in these structures because they have nearly no periodicity-induced reflection.

The band structure is unusual in a second way. The coupling at the waveguide-crossing points is not (only) a standard reactive, i.e. power-exchange, coupling that results from index perturbations, but includes radiative interference coupling that scatters light from both the 1<sup>st</sup> and 3<sup>rd</sup> order transverse modes. This means there is a propagation constant splitting that is not real, but imaginary (or, more generally complex when the standard index perturbation part is also accounted), and leads to one Bloch mode with a low imaginary part of the complex propagation constant (low loss), and another with a high loss. There are analogous frequency eigenstates in resonators based on similar physics [18, 19].

Physically, the low-loss Bloch mode corresponds to a superposition of modes 1 and 3 of the unperturbed waveguide with the right ratio of amplitudes to produce a field minimum (or null) at the scattering points. The high-loss mode in turn has constructive interference at these points. To realize a low-loss crossing array, the objective is to choose the waveguide cross-sectional dimensions, and crossing periodicity, that minimize the loss of the lower loss Bloch mode. This insight also applies to the design of single crossings [10, 13, 14].

To arrive at a low-loss Bloch mode, our strategy is to maximize the imaginary splitting of the propagation constants for a *given* scatterer geometry. Radiation loss through scattering provides an imaginary part to the propagation constants [dashed arrow, Fig. 2(a)], while radiative splitting brings back the low-loss mode down to as close to zero loss as the geometry permits via radiative cancellation [split arrows, Fig. 2(a)]. As with real splitting, the maximum splitting occurs at the phase matching condition. In our case, a periodic perturbation is required to match the difference in propagation constants of modes 1 and 3,  $\Lambda = 2\pi/(\beta_1 - \beta_3)$ . Since  $\beta_1$  and  $\beta_3$  are eigenstates of the unperturbed waveguide without crossings, rigorous simulations that account for self-coupling perturbations [20] in the crossings lead to a small correction to the periodicity in the actual design.

If the fundamental mode is launched into the multimode guide [Fig. 2(b)], the first few crossings strongly scatter until the low-loss wave is established. The incident mode 1 field can be thought of as a superposition of the low-loss and high-loss Bloch waves with mode 1 components adding and mode 3 components canceling. As the high-loss Bloch mode decays with a fast decay rate, only the low loss, breathing mode remains. We can observe the fraction of mode 1 and 3 present in a cross-section where the low-loss wave has converged to a steady state. If this ratio of modes 1 and 3 is excited at the start of the structure in Fig. 2b (as is done in Fig. 1), no power needs to be initially coupled to the high-loss Bloch wave, and thus no scattering will occur at the first few crossing points.

For efficient excitation of the low-loss Bloch wave from a single mode waveguide, we employ a symmetric, non-adiabatic taper. It acts as a “directional coupler” between modes 1 and 3 of the multimode guide [10, 12, 13] (by symmetry there is no coupling to asymmetric mode 2). Another approach, MMI excitation at an abrupt junction [11], is equivalent to the non-adiabatic taper design in the (non-optimal) limit of zero taper length.

Devices for experimental demonstration were designed to be implemented in the 220 nm silicon device layer ( $n = 3.476$  at 1550 nm wavelength) of a standard silicon photonics silicon-on-insulator (SOI) platform with a  $2\ \mu\text{m}$  oxide undercladding, and oxide overcladding ( $n = 1.45$ ). The width is chosen to sufficiently confine the first and third modes, without admitting a 5<sup>th</sup> mode. Dimensions are given in Fig. 3c, with the period obtained from a parameter sweep in 3D FDTD simulations to provide the minimum loss per crossing.

Figure 3a shows 3D FDTD simulations of a linear taper design, showing coupling to mode 3, and corresponding radiative loss. For an optimum mode 3 coupling ratio of just under 5%, a  $1.35\ \mu\text{m}$  taper suffices, and the radiation loss is negligible ( $<0.4\%$ ) so we didn’t consider more complex taper shapes. The taper in Fig. 3a is broadband, with 4.75% coupling at 1550 nm, a 0.3% variation over 1450–1550 nm, increasing to 6% at 1650 nm.

Figure 3b shows the simulated transmission spectra of

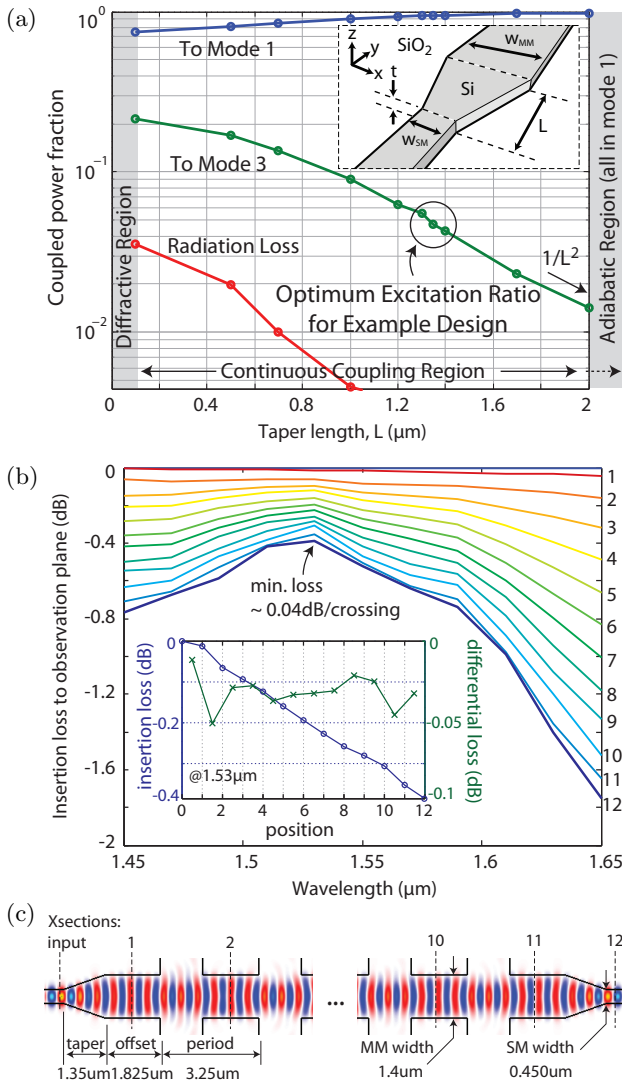


Fig. 3: Crossing design: (a) short, non-adiabatic symmetric taper as a directional coupler between the 1<sup>st</sup>- and 3<sup>rd</sup>-order modes, allowing efficient excitation of a breathing Bloch mode of the crossing array; coupling and loss vs. length. (b) Simulated transmission after 1-10 crossings, and through entire structure including tapers (3D FDTD). (c) Field from a monochromatic 3D FDTD simulation at 1550 nm.

a complete waveguide crossing array with 10 crossings and input/output tapers to 450-nm-wide, single mode waveguides. The insertion loss vs. wavelength is computed after 1–10 crossings, with observation planes labeled in Figs. 3b (right) and 3c, and through the entire structure including tapers, using 3D FDTD. Peak theoretical transmission is  $\sim 0.4$  dB for 10 crossings and two tapers, and  $\sim 0.033$  dB average per added crossing (Fig. 3b inset). Figure 3c shows the transverse electric field distribution in the structure designed to excite the low-loss Bloch wave from a single mode input guide at 1550 nm. The input taper must be placed at a particular offset from the first crossing in order for the first “focal point” of the field envelope to coincide with the first crossing waveguide.

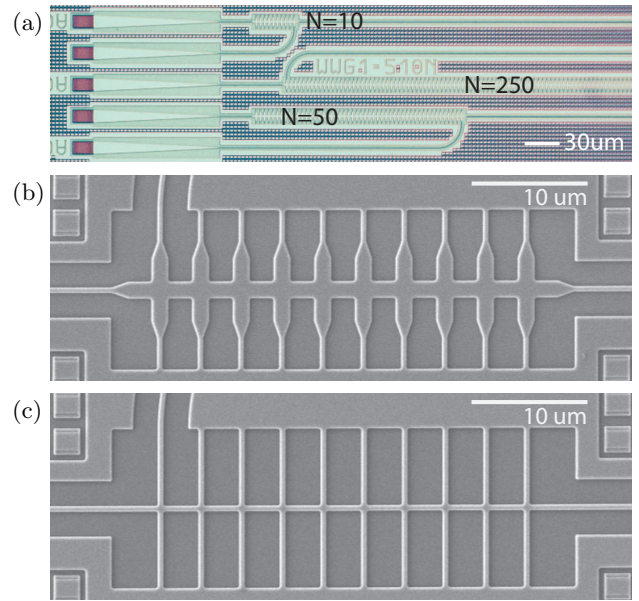


Fig. 4: (a) Optical micrograph of on-chip crossing arrays fabricated through IMEC/ePIXfab [21] with 10, 250 and 50 periods. (b) SEM of a 10-period low-loss Bloch crossing array. (c) SEM of a 10-period normal crossing array.

Arrays with  $N = 10, 50, 150$  and 250 crossings were realized. Fig. 4a shows a typical set of on-chip devices, fabricated through the ePIXfab multiproject wafer service [21]. To pre-compensate for bias in the lithography, the width of the multimode waveguide section was varied in layout from 1450 nm to 1510 nm, with other dimensions remaining at design target (Fig. 3c). Figures 4b and 4c show scanning electron micrographs (SEMs) of a Bloch-wave 10-crossing array and a “normal” 10-crossing array based on 450-nm-wide single mode waveguides.

Figure 5a shows measured total insertion loss normalized to include losses from the non-adiabatic tapers and the crossings, relative to a plain single mode waveguide. For each waveguide width variant, the slope of insertion loss versus number of crossings gives the loss per crossing (not including the tapers) at each wavelength (linear fits, see Fig. 5a inset, give Fig. 5b). A device with waveguide width 1510 nm shows an average loss per crossing of 0.04 dB at  $\lambda = 1505.8$  nm. The flatter loss slope of the last 100 crossings (Fig. 5a, inset) shows loss of 0.032 dB/crossing with  $\pm 0.005$  dB uncertainty due to coupling (equivalent to  $\sim 100$  dB/cm distributed loss). The demonstrated loss matches theory closely, but the minimum loss wavelength is shifted down by about 25 nm. This is consistent with an error in device layer thickness/width. For small shifts, the minimum insertion loss is not substantially changed.

At the 250-crossing Bloch array’s optimal wavelength (Fig. 6a), it has lower insertion loss than a 10-crossing single-mode array. Figure 6b shows the transmission and crosstalk of a 1510 nm-wide 10-crossing Bloch-wave design and a 10-crossing single-mode array. Apart from 13 dB higher transmission, approaching sub-1% loss per



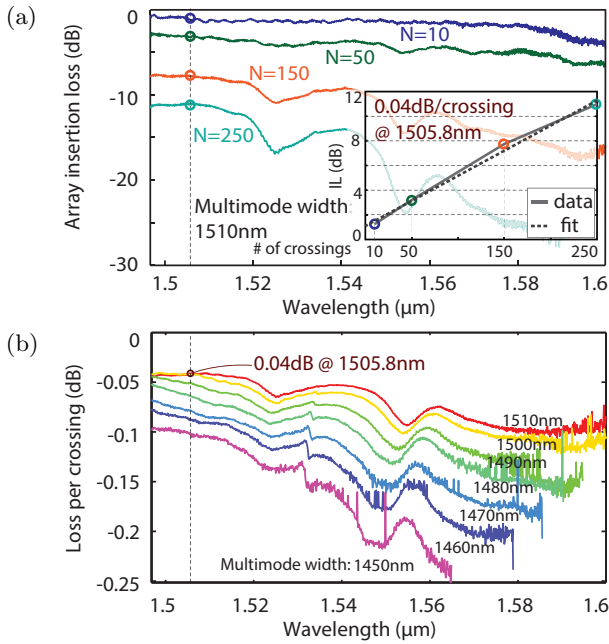


Fig. 5: (a) Spectral insertion loss of Bloch arrays with 10, 50, 150 and 250 crossings (1510 nm width); (b) insertion loss/crossing vs. wavelength of crossing arrays with waveguide widths from 1450 nm to 1510 nm.

crossing, the Bloch-wave crossing array also suppresses crosstalk by at least 35 dB (limited by measurement noise), 20 dB more than a normal crossing array. This is consistent with the theoretical prediction [12].

The experimental demonstration of CMOS compatible waveguide crossing arrays with ultra-low losses, matching theory, may be enabling and impact photonic network-on-chip architecture. These structures offer capabilities for electrically/thermally active, suspended and optomechanical photonic structures with minimized scattering loss. More generally, this concept extends to higher order, as well as transversely asymmetric structures [13, 22], as recently applied in modulators [23]. This work was supported by NSF award ECCS-1128709.

## References

- [1] C. Batten, A. Joshi, J. Orcutt, A. Khilo, B. Moss, C. Holzwarth, M. Popović, H. Li, H. Smith, J. Hoyt, F. Kärtner, R. Ram, V. Stojanović and K. Asanović, *IEEE Micro*, **29**, 8-21 (2009).
- [2] T. Fukazawa, T. Hirano, F. Ohno and T. Baba, *Jap. J. Appl. Phys.* **43**, 646 (2004).
- [3] T. Barwicz, M.R. Watts, M.A. Popović, P.T. Rakich, L. Succi, F.X. Kärtner, E.P. Ippen and H.I. Smith, *Nat. Photon.* **1**, 57 (2007).
- [4] M.R. Watts, Ph.D. Thesis, MIT, Cambridge, MA, 2005.
- [5] C. Manolatou, S.G. Johnson, S. Fan, P.R. Villeneuve, H.A. Haus and J.D. Joannopoulos, *J. Lightwave Technol.* **17**, 1682 (1999).
- [6] Y. Yu, M. Heuck, S. Ek, N. Kuznetsova, K. Yvind and J. Mørk, *Appl. Phys. Lett.* **101**, 251113 (2012).
- [7] W. Bogaerts, P. Dumon, D.V. Thourhout, D. Taillaert, P. Jaenen, J. Wouters, S. Beckx, V. Wiaux and R. Baets, *IEEE J. Sel. Top. Quantum Electron.* **12**, 1394 (2006).

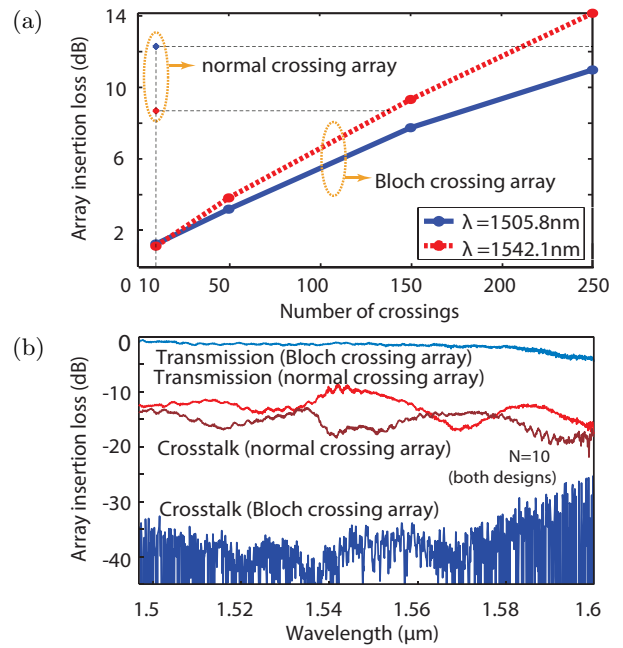


Fig. 6: (a) Insertion loss vs. number of crossings in Bloch crossing array (width 1510 nm) and a 10-crossing normal array, at  $\lambda = 1505.8$  nm where the Bloch crossing has the lowest loss and at  $\lambda = 1542.1$  nm where the normal crossings have the lowest loss. (b) Transmission and crosstalk spectra of the Bloch and normal crossing arrays with 10 periods.

- [8] A. Jones, C. DeRose, A. Lentine, D. Trotter, A. Starbuck, and R. Norwood, *Opt. Express* **21**, 12002 (2013).
- [9] H.R. Stuart, *Opt. Lett.* **28**, 2141 (2003).
- [10] H. Liu, H. Tam, P.K.A. Wai and E. Pun, *Opt. Commun.* **241**, 99 (2004).
- [11] H. Chen, A.W. Poon, *IEEE Photon. Technol. Lett.* **18**, 2260 (2006).
- [12] M.A. Popović, E.P. Ippen and F.X. Kärtner, in *Proc. Annual Meeting of IEEE Lasers and Electro-Optics Society (LEOS)*, Oct 2007, paper MF5.
- [13] M.A. Popović, U.S. Pat. 7,903,909 and 8,116,603 (2007).
- [14] Y. Zhang, S. Yang, A.E.-J. Lim, G. Lo, C. Galland, T. Baehr-Jones and M. Hochberg, *IEEE Photon. Technol. Lett.*, **25**, 422 (2013).
- [15] G. Goubau and F. Schwering, *IEEE Trans. Antennas Propagat.* **9**, 248 (1961).
- [16] Y. Liu, J. Shainline, X. Zeng and M.A. Popović, in *Integrated Photonics Research*, July 2013, paper IM1A.4.
- [17] Y. Zhang, A. Hosseini, X. Xu, D. Kwong, and R. Chen, *Opt. Lett.* **38**, 3608 (2013).
- [18] M.S. Dahlem, C.W. Holzwarth, H.I. Smith, E.P. Ippen and M.A. Popović, in *Proc. Integrated Photonics Research*, July 2010, paper IMC4.
- [19] C. Gentry and M. Popović, in *CLEO: 2013, OSA Technical Digest*, June 2013, paper CM3F.1.
- [20] M.A. Popović, C. Manolatou and M.R. Watts, *Opt. Express*, **14**, 1208 (2006).
- [21] ePIXfab, www.epixfab.eu.
- [22] Y. Liu, X. Zeng, J. Shainline, and M.A. Popović, in *Integrated Photonics Research*, July 2013, paper IM2B.6.
- [23] J.M. Shainline, J.S. Orcutt, M.T. Wade, K. Nammari, O. Tehar-Zahav, Z. Sternberg, R. Meade, R.J. Ram, V. Stojanović and M. Popović, *Opt. Lett.* **28**, 2729 (2013).